

# Modeling reactivity insertion experiments of TRISO particles in NSRR using BISON

D. Schappel<sup>a,\*</sup>, N.R. Brown<sup>b,a</sup>, K.A. Terrani<sup>a</sup>

<sup>a</sup> Oak Ridge National Laboratory, Oak Ridge, TN, United States

<sup>b</sup> University of Tennessee, Knoxville, TN, United States

## ARTICLE INFO

### Article history:

Received 26 November 2019

Received in revised form

17 December 2019

Accepted 19 December 2019

Available online 20 December 2019

### Keywords:

NSRR

TRISO

BISON

Reactivity

Silicon carbide

Fracture

## ABSTRACT

This research presents BISON simulations of stress, temperature, and failure probability of tristructural isotropic (TRISO) fuel particles subjected to transient power pulse conditions in the Nuclear Safety Research Reactor (NSRR). By modifying the default elastic properties of the PyC and the UO<sub>2</sub> coefficient of thermal expansion correlation, BISON was found to produce suitable agreement with the observed and independently simulated results when appropriate shape and scale Weibull parameters for SiC failure were chosen. The Weibull parameter effects were also explored within the range of SiC failure and were applied using experimental data from hemispherical crush testing.

Published by Elsevier B.V.

## 1. Introduction

Tristructural isotropic (TRISO) fuel particles have long been developed for gas-cooled reactors [1,2]. Because of their excellent fission product retention capability [3,4], they are being considered for a wide range of advanced reactor designs. The fuel particles consist of a uranium-bearing fuel kernel surrounded by a low-density carbon buffer layer, a dense inner pyrocarbon (IPyC) layer, a SiC coating layer, and an outer pyrocarbon (OPyC) layer. Under a short-duration reactivity-initiated accident (RIA), as energy is rapidly deposited in the fuel kernel, it may experience rapid expansion and melting, which damages and fractures the PyC and SiC coating layers responsible for fission product retention. This work focused on modeling the behavior of the individual TRISO particles using the BISON [5] fuel performance tool and comparing the results with historical transient experimental data and calculations from the literature. This work considers two failure mechanisms: kernel melting and fracture of the SiC coating layer primarily due to the kernel's thermal expansion.

Depending on the size of the reactivity insertion and the

duration of the resulting power pulse, the temperature of the kernel can exceed its melting temperature [6]. Most of the material models available for TRISO fuel performance modeling are designed to target normal operating conditions and transients that do not result in temperatures close to fuel melting (i.e., pressurized or depressurized conduction cooldown), or <2,073 K. In this study, the BISON tool was used to model experiments on single fuel particles performed by Umeda et al. [6] that result in much higher temperatures. The goal was to assess and subsequently improve the predictive capability of this fuel performance modeling tool. This is consistent with the accelerated fuel development and qualification process suggested by Terrani [7], which strives to leverage an agile and iterative combination of integral fuel performance modeling with separate effects testing.

The Nuclear Safety Research Reactor (NSRR) has a much shorter power pulse width than most reactors designed to be fueled by TRISO particles; this increases kernel temperatures leading to potential melting and increased probability for fuel particle failure as the kernel thermally expounds compared with equivalent energy depositions from reactors with longer pulses. This short pulse is driven by the very small neutron generation time of that reactor compared with a typical graphite-moderated modular high-temperature gas-cooled reactor (mHTGR). BISON was originally designed and largely benchmarked against quasi steady-state

\* Corresponding author.

E-mail address: [schappeldp@ornl.gov](mailto:schappeldp@ornl.gov) (D. Schappel).

simulations. Comparing this set of highly transient experiments allows the selected models and simulation setup to be validated, which gives confidence in BISON's ability to predict other transients of similar or somewhat longer timescales.

The typical initiating event for an RIA in an mHTGR is a control rod withdrawal (CRW) or an increase in cooling on the secondary side. Data for such hypothesized events exist in the literature for several designs, including the pebble bed modular reactor (PBMR) 268 MW and 400 MW designs, the General Atomics mHTGR-350 design, and the High-Temperature Reactor Pebble Bed Module (HTR-PM) design and demonstration plant. Actual CRW tests were performed recently at two small-scale mHTGR engineering demonstration reactors: the 10 MW High-Temperature Gas-Cooled Reactor-Test Module (HTR-10) in China and the High-Temperature Engineering Test Reactor (HTTR) in Japan.

Table 1 shows several examples from the literature. The table lists the reactor design or the actual reactor, along with the type of mHTGR (prismatic compact-based or pebble-based fuel), the category of data (calculation or experiment), the initiating event for the accident simulation or test, the estimated fuel kernel energy deposition (based on available fuel temperature data from the reference), and whether the source contains explicit neutronics modeling of the fuel kernels or uses a homogenized fuel model. The key takeaway from these data is that kernel energy deposition in mHTGR RIAs is expected to be less than the lowest fuel kernel energy deposition (578 J/g) in the fuel during the NSRR experiments. Explicit neutronics modeling of the fuel kernel will decrease this energy deposited due to enhanced feedback from the near-adiabatic nature of the fast transient [8].

## 2. Experimental data

The experimental data and calculations were published by Umeda et al. [6]. The experiments were performed in the NSRR in Japan. The reactor is a 20% enriched U–ZrH fueled with ZrH and a water moderator. The maximum reactivity insertion is listed at \$4.7 and a peak power of 23 GW thermal (GWth) [24]. However, the width of the power pulses decreases with increasing reactivity insertion [25]. Data from Nakamura et al. and Saito et al. [25,26] were used to generate and validate a point kinetics model with linear thermal feedback to produce the estimated power pulse shape boundary conditions for the TRISO experiments. The power during the transients was calculated using point kinetics with six groups of delayed neutrons [25] and first-order heat transfer through the volume resistance of the fuel, with reactivity feedback

given by Eq. (1):

$$\delta\rho(t) = \gamma \int_0^t [P(t') - P_0] \exp[-\lambda_H(t - t')] dt' \quad (1)$$

where  $\delta\rho(t)$  is the reactivity feedback following the imposed reactivity,  $\gamma$  is the energy Doppler feedback coefficient,  $t$  is elapsed time,  $P(t') - P_0$  is the change in power, and  $\lambda_H$  is the time constant of the heat transfer through the fuel and into the coolant. These pulses are shown in Fig. 1, and the NSRR natural pulse is compared with the natural pulses of other reactors in Fig. 2 [27]. Three important quantities were validated in the kinetics models by comparing them with NSRR historical data: pulse width, pulse magnitude, and asymptotic power after the pulse. The validation calculation was performed for an insertion of \$3.13 [25,26], which is in the correct range for the four reactivity insertions in the Umeda et al. [6] experiments.

The geometry and layer density of the TRISO particles is presented in Umeda et al. [6] and listed in Table 2. Seven unirradiated particles were placed in a graphite ring which had a 10 mm outer diameter, a 4 mm inner diameter, and a 3 mm height. Thirty-six rings were placed in each fuel segment, and two segments were used in each test, as shown in Fig. 3. Eight segments were tested with energy depositions ranging from 578 to 1,869 J/g UO<sub>2</sub> [6].

The results of the experiments showed intact particles for the

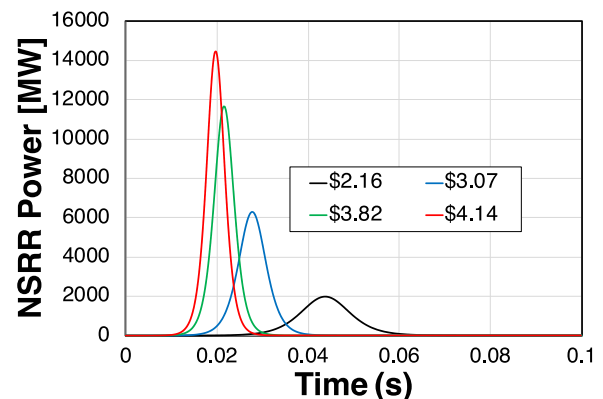


Fig. 1. Plot showing the pulses used in the NSRR TRISO fuel RIA condition experiments.

Table 1

Example of mHTGR RIA initiating events and estimated fuel kernel energy depositions from the literature.

Ref.	Reactor system	Type of mHTGR	Category of data	Event	Estimated fuel kernel energy deposition (J/g)	Explicit modeling of kernel
[9]	PBMR-268	Pebble	Calculation	Single control rod ejection	10–25 (max)	No
[10]	PBMR-268	Pebble	Calculation	Increase in cooling on secondary side	50 (max)	No
[11]	mHTGR-350	Prismatic	Calculation	Total CRW, no SCRAM	250–350 (average)	No
[12,13]	HTR-10	Pebble	Experiment and calculation	Partial CRW test	10–15 (max)	No
[14]	HTR-10	Pebble	Calculation	CRW accident	50–70 (max)	No
[15]	mHTGR-350	Prismatic	Calculation	Partial CRW accident	10–15 (max)	No
[16]	HTTR	Prismatic	Experiment and calculation	Partial CRW test	2–3 (average)	No
[17]	PBMR-400	Pebble	Calculation	Total control rod ejection, no SCRAM	90–120 (max)	Yes
[18]	PBMR-400	Pebble	Calculation	CRW	50–110 (max)	Yes
[19]	PBMR-400	Pebble	Calculation	Total control rod ejection, no SCRAM	50–70 (max)	Yes
[20,21]	PBMR-400	Pebble	Calculation	Total control rod ejection, no SCRAM	225–300 (max)	No
[22]	PBMR-268	Pebble	Calculation	Total control rod ejection, no SCRAM	100–250 (max)	No
[23]	HTR-PM	Pebble	Calculation	CRW accident	30–85 (max)	No

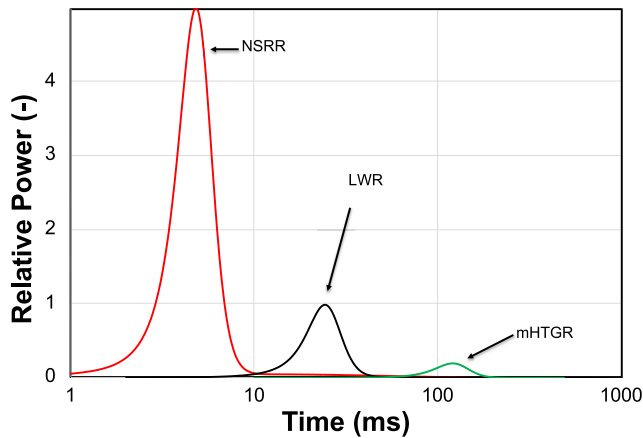


Fig. 2. Comparison of the NSRR natural pulse to pulses of other reactors.

Table 2

List of the TRISO geometry and densities [6].

Layer	Thickness ( $\mu\text{m}$ )	Density ( $\text{kg/m}^3$ )
UO <sub>2</sub> kernel	500 diameter	10,630
Buffer	95	1,050
IPyC	40	1,850
SiC	35	3,190
OPyC	40	1,850

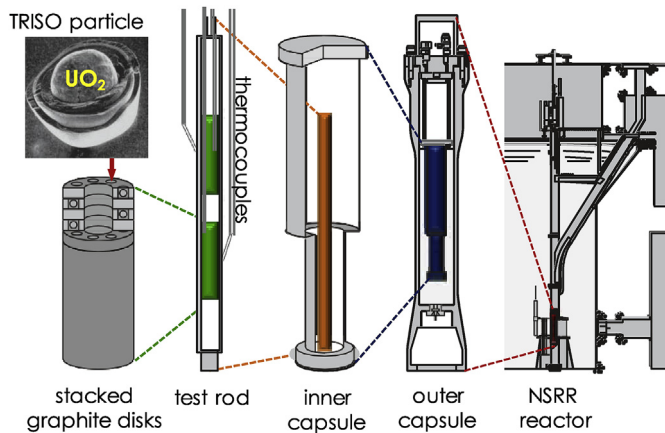


Fig. 3. General NSRR TRISO irradiation setup. Adapted from Umeda et al. [6].

578 J/g case, kernel cracking in the 695 J/g through 1,254 J/g cases, and rapidly increasing particle failure fractions for 1,436 J/g and higher-energy depositions. Fuel melting was also observed in the 1,254 J/g and higher-energy deposition cases [6].

### 3. BISON and material models

BISON is a finite element code developed and maintained by Idaho National Laboratory (INL). BISON is based on the MOOSE [28] computational framework and uses LIBMESH [29] and PETSc [30] to perform the numerical solutions. BISON has been used to perform TRISO simulations of operating and high temperature conditions [31]. However, this work focuses on the transient and high-temperature nature of the selected NSRR experiments.

Since the fuel used in the NSRR experiments was unirradiated and experienced short-duration pulses, irradiation models such as

irradiation induced dimensional change (IIDC) of the carbon materials, swelling, and irradiation creep are not included in these simulations. The primary material properties are specific heat, thermal expansion, thermal conductivity, density, and elastic modulus. Table 3 lists the mechanical properties that were modeled as constants in the simulations.

The Poisson's ratios were set according to default values in the BISON TRISO example files. However, some modifications were made to the elastic moduli. The UO<sub>2</sub> elastic modulus was decreased from 200 to 170 GPa as a porosity correction based on data from Eq. (7) in Cappia et al. [33]. The elastic modulus of the SiC coating layer was also decreased from 450 to 430 GPa as a porosity correction based on Eq. (17) in Snead et al. [34]. The elastic modulus of PyC was decreased to 29 GPa, and the buffer was reduced to 7 GPa based on the Forschungszentrum Julich (FZJ) recommendations for unirradiated PyC [35]. The elastic modulus for the graphite matrix was set to 10 GPa as an approximation based on the information in the Graphite Design Handbook [32].

#### 3.1. Thermal conductivity

The unirradiated UO<sub>2</sub> thermal conductivity is given by equations in Fink [36]. The thermal conductivity is capped at 2,670 K per recommendation from Fink [36]. Although UO<sub>2</sub> melts at about 3100 K, which is less than the maximum temperature in Fig. 4, the BISON model does not have a separate set of material properties for melted conditions. Since the estimated kernel temperatures in the NSRR experiments exceed 3,100 K, displaying the material property predictions above the melting temperature is relevant. Fig. 4 plots the unirradiated thermal conductivity of the UO<sub>2</sub> and SiC versus temperature.

The thermal conductivity of the unirradiated chemical vapor deposition (CVD)-SiC coating layer was set to Eq. (12) in Snead et al. [34], where the unirradiated thermal conductivity is inversely proportional to temperature with values of about 350 to 50 W/m-K.

The thermal conductivity of PyC is dependent on the porosity and is given by Eq. (2) [37]:

$$k = 19.9866 \frac{1 - P}{1 + 9P} \quad (2)$$

where  $P$  is the porosity (–), and  $k$  is the thermal conductivity in (W/m-K). The values are in the range of about 4 W/m-K for PyC and about 0.7 W/m-K for buffer. The graphite thermal conductivity data are from Li et al. [38]. The unirradiated trend is inversely proportional to temperature, with values between about 60 and 100 W/m-K.

#### 3.2. Specific heat

The specific heat of UO<sub>2</sub> is given by an equation from Fink et al. [36] and is also capped at 2,670 K. Fig. 5 shows a plot of the UO<sub>2</sub> and SiC specific heats. The specific heat of SiC was set to Eq. (10) in Snead et al. [34], which is capped at 2,400 K.

The specific heat of buffer, PyC, and graphitic matrix was set to a

Table 3

List of the mechanical properties used for the TRISO particles [31–35].

Material	Elastic modulus (GPa)	Poisson's ratio (–)
UO <sub>2</sub>	170	0.345
Buffer	7	0.3
PyC	29	0.3
SiC	430	0.18
Graphitic matrix	10	0.3

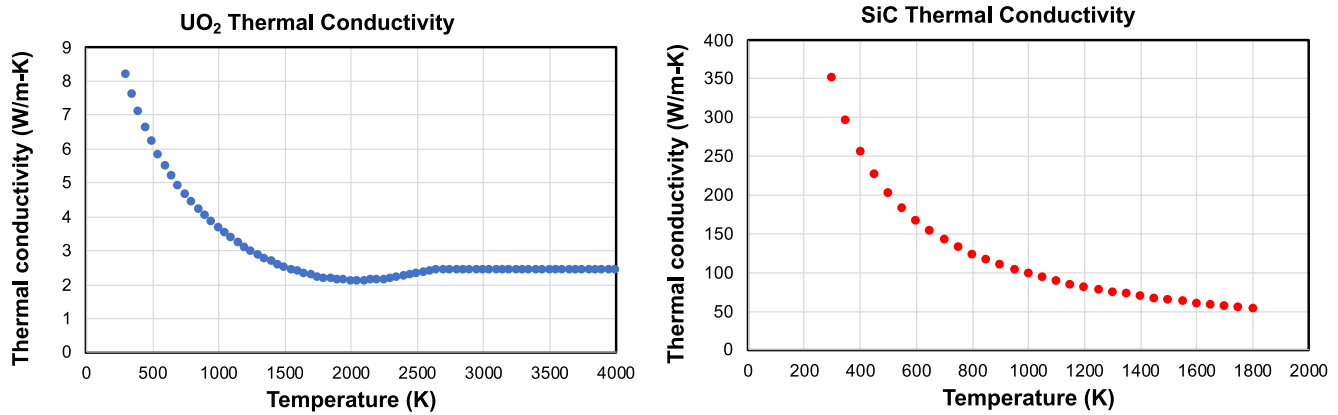


Fig. 4. Plot of the unirradiated UO<sub>2</sub> (left) and SiC (right) thermal conductivity to high temperature.

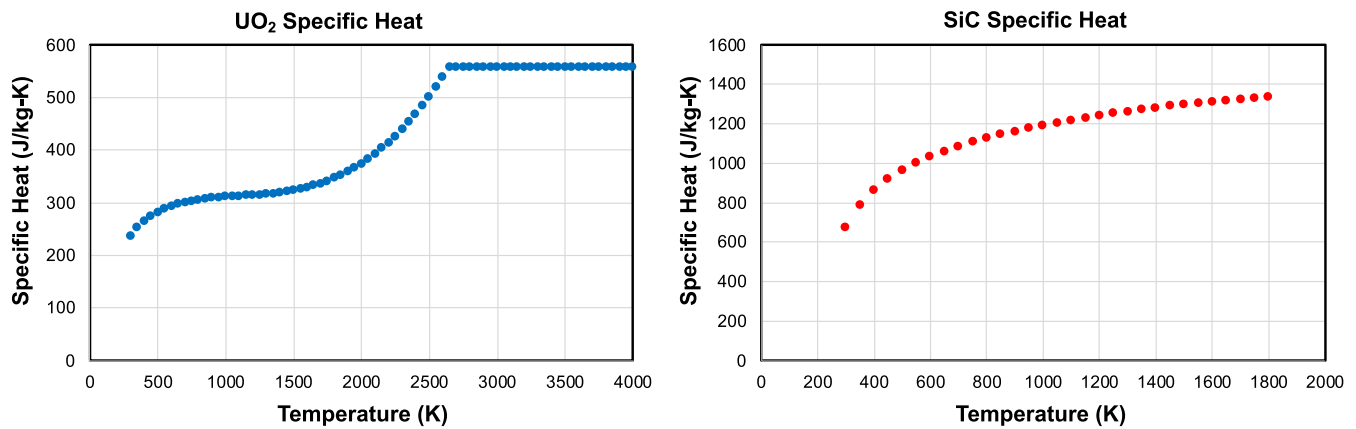


Fig. 5. Plot of the UO<sub>2</sub> (left) and SiC (right) specific heat.

constant 720 J/kg-K, which is a typical average value for carbon materials.

### 3.3. Coefficient of thermal expansion

The coefficient of thermal expansion (CTE) of UO<sub>2</sub> was set to a correlation from MATPRO [39], which gives a smaller value at high temperatures than the piecewise correlation from Martin [40]. The SiC CTE was set to Eq. (16) in the SiC Handbook [34], which increases rapidly with temperature and is capped at  $5 \times 10^{-6}/K$  at about 1,000 K. Fig. 6 plots the CTEs vs. temperature.

The CTE of PyC and the buffer were set to  $5.6$  and  $3.5 \times 10^{-6}/K$  per UK recommendations [35], which are very similar to FZJ recommendations ( $5.5$  and  $3.5 \times 10^{-6}/K$ ).

## 4. Model description

The simulations consisted of a single TRISO particle surrounded by a 325  $\mu m$  thick graphite shell that acted as an approximate heat sink for the particle. The outer surface of the graphite shell was assumed to be adiabatic due to the short pulse duration, with an initial temperature of 373 K. The stress-free temperature was set to 1,873 K as an estimate of the SiC coating layer deposition temperature. This resulted in the SiC layer initially being in compression due to the larger CTE of the PyC layers and UO<sub>2</sub> compared with the SiC layer. In these simulations, interface debonding was not

permitted.

A 3D mesh was used in these simulations. Originally, some consideration for aspherical effects given, but was decided against due to reasonable agreement between the symmetric simulations and the experimental results. The approximate mesh size for the particles was about 10  $\mu m$  radially and about 100  $\mu m$  on the circumferential directions. Further refining the mesh produced diminishing returns for the accuracy of the results. The simulation was run at the initial condition for 10 s, and then the reactivity insertion began. The simulation was stopped 1 s after the initiation of the transient, and 0.5 ms timesteps were used during the transient. Further reducing the timestep size to 0.05 ms did not significantly change the resulting stresses. Thus, the 0.5 ms timesteps were considered satisfactory.

## 5. Results

Fig. 7 shows the power and energy deposition vs. the time, starting with the initiation of the transient. The full width half max of the pulse is about 10 ms for the smaller 578 and 695 J/g cases and decreases to about 4 ms for the 1,642 and 1,869 J/g cases.

Fig. 8 compares the maximum kernel temperatures that were calculated in ABAQUS [6] and the BISON results from this work. The BISON results predict larger maximum temperatures at the lower energy depositions but predict smaller temperatures for the largest energy depositions. The most likely primary cause of the

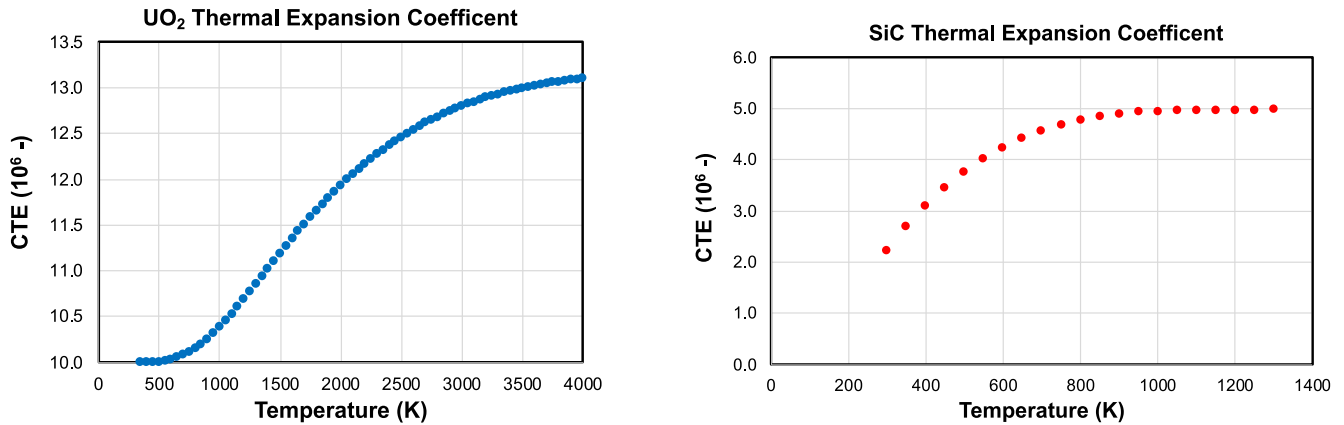


Fig. 6. Plot of the  $\text{UO}_2$  (left) and SiC (right) CTE.

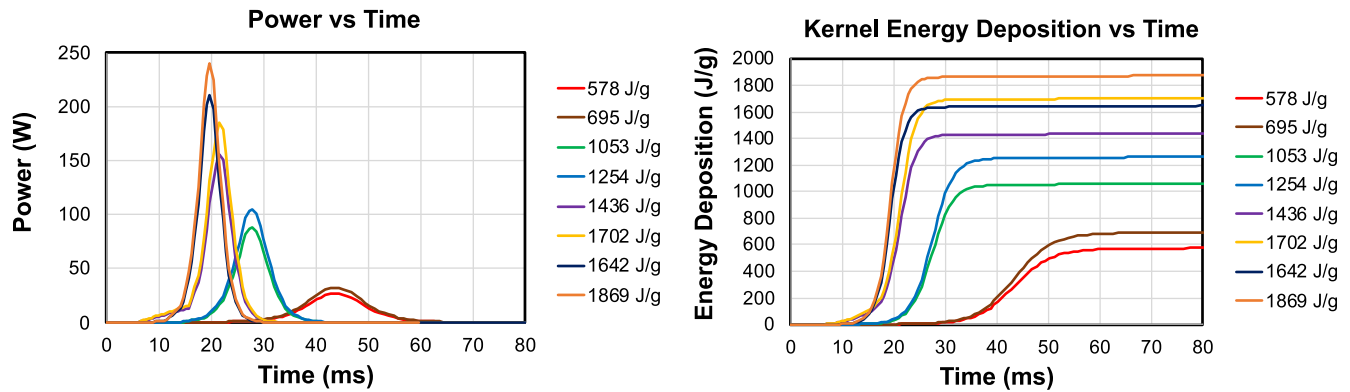


Fig. 7. Plots of the power (left) and energy deposition (right) for the simulated NSRR conditions.

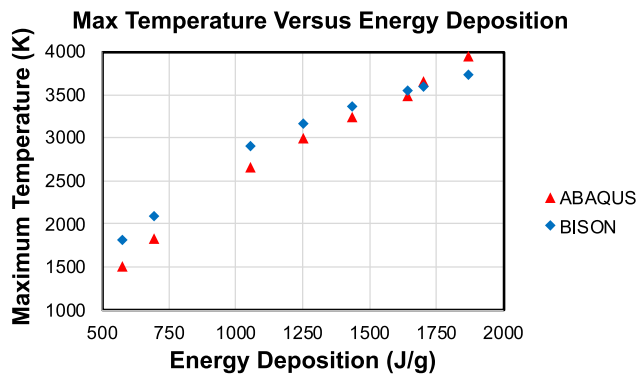


Fig. 8. Comparison of the maximum temperatures calculated by Umeda et al. in ABAQUS [6] and this work in BISON.

temperature differences is the specific heat correlation of the  $\text{UO}_2$ . However, this is speculation since the material property selection for the ABAQUS simulations was not published [6], and thus the modeling differences between the two models remains unclear. Considering the situation, reasonable agreement for fuel performance codes was obtained in maximum temperature, and the resulting hoop stresses follow the difference in thermal expansion from the kernel compared with the SiC layer. This is expected, since

the kernel has over twice the CTE of the SiC. Additionally, the PyC has a somewhat larger CTE than the SiC. The maximum temperatures of the kernels, the temperatures of the SiC layers, and the hoop stress in the SiC layers are plotted in Fig. 9.

The gray line in Fig. 9 denotes the estimated melting temperature of  $\text{UO}_2$ . The heat of fusion and subsequent gas pressure from vaporized fuel is not included in the model. Thus, the temperatures and stresses above the melting temperature of  $\text{UO}_2$  may be considerably different from those predicted by the model.

The SiC layer is initially in compression because the initial temperature is 373 K, and the stress-free temperature was set to the estimated deposition temperature of 1,873 K. This prevents the 578 and 695 J/g cases from predicting tensile hoop stresses, which seems to be somewhat reasonable since no fractures were observed in these cases. However, as the energy deposition increases, the stress becomes great enough that SiC fracture is predicted.

The microstructure and strength of the SiC coating layer of the fuel particles that was used in these experiments is unknown beyond what is reported in Umeda et al. [6] and other generic reports from the Japanese HTTR program [41]. However, the range of fracture strength in SiC coating layers of TRISO fuel particles has been experimentally assessed and could be used to calculate the cumulative failure probabilities of the SiC layers in this study. The cumulative failure probability of the SiC layer using Weibull statistics is given in Eq. (3),



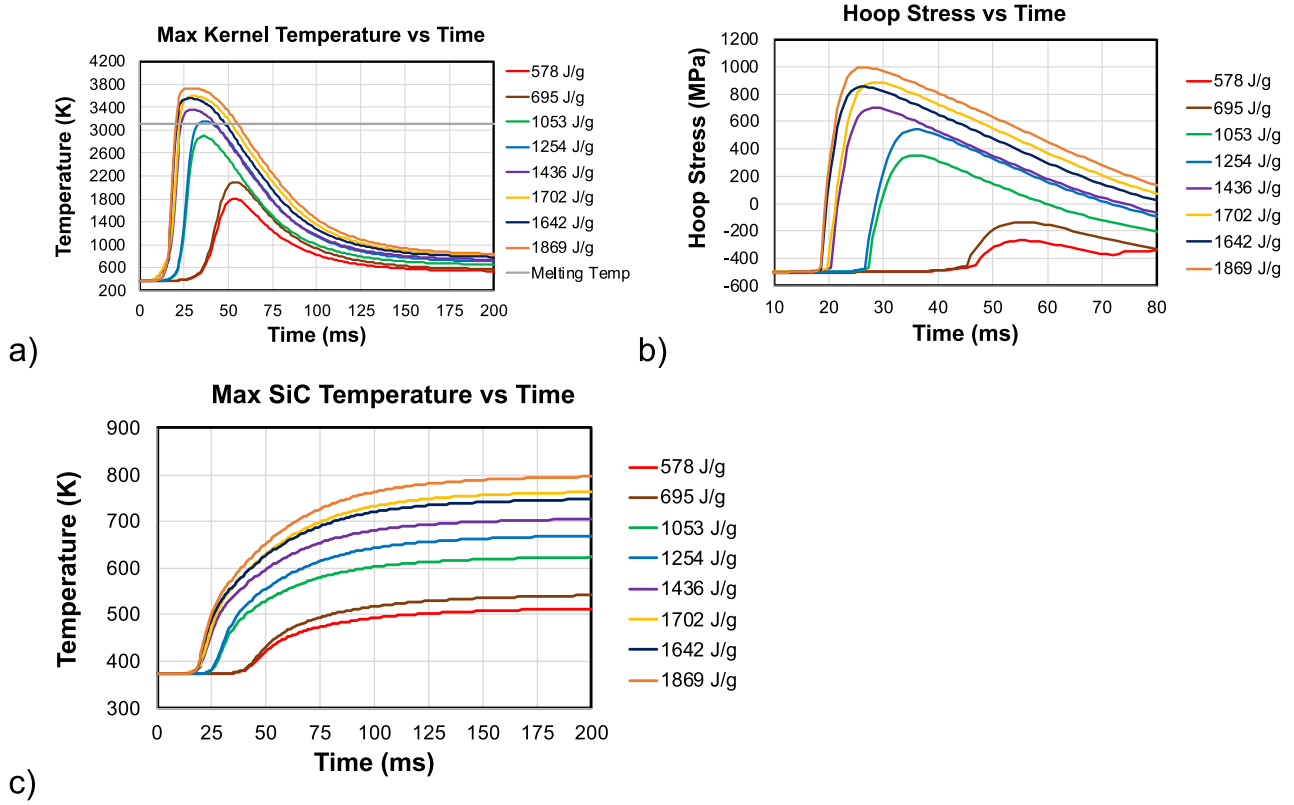


Fig. 9. (a) Maximum kernel temperature vs. time, (b) hoop stress on the inner surface of the SiC layer vs. time, and (c) maximum SiC temperature vs. time.

$$F_p = 1 - \exp \left[ - \int \frac{(\sigma_{mp1}^m + \sigma_{mp2}^m + \sigma_{mp3}^m)}{V_c \sigma_0^m} dV \right] \quad (3)$$

where  $F_p$  is the cumulative failure probability (–) of the SiC layer, and  $V_c$  ( $m^3$ ) is the characteristic volume of the test samples that were used to extract Weibull parameters. Those parameters are the characteristic strength,  $\sigma_0$  (MPa), and the Weibull modulus,  $m$ .  $\sigma_{mp}$  (MPa), is the calculated principal stress in the various directions that is then integrated over the volume of the SiC coating layer.

The maximum principal stresses are used because SiC is a brittle material that is expected to fail due to normal stresses. The principal stresses are found by rotating the stress tensor until the shear stresses are zero, thereby providing a generalized method for calculating the normal stresses. However, in this spherically symmetric case, the differences between the max principal and hoop stresses are usually less than 1 MPa.

The characteristic volume of the sample from which the characteristic strength was determined is included because the failure of brittle materials begins at a flaw, and larger samples or simulated volumes have an increased likelihood of containing a flaw. This allows for a volume normalization that does not depend on the number of elements in the mesh and allows for the test samples that provide the basic material property to have different volumes than the simulated geometry under stress.

Experimental fracture testing data on SiC coating layers of TRISO fuel particles is available in the literature [42–48]. Strength of several SiC coating layers resulting from different CVD conditions were evaluated in studies Hunn et al. [48]. The fracture tests were performed on SiC hemispheres, as shown in Fig. 10. A segment of the resulting strength data from Hunn et al. [48] is shown in a

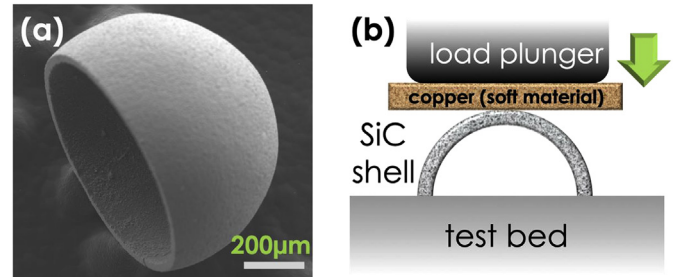
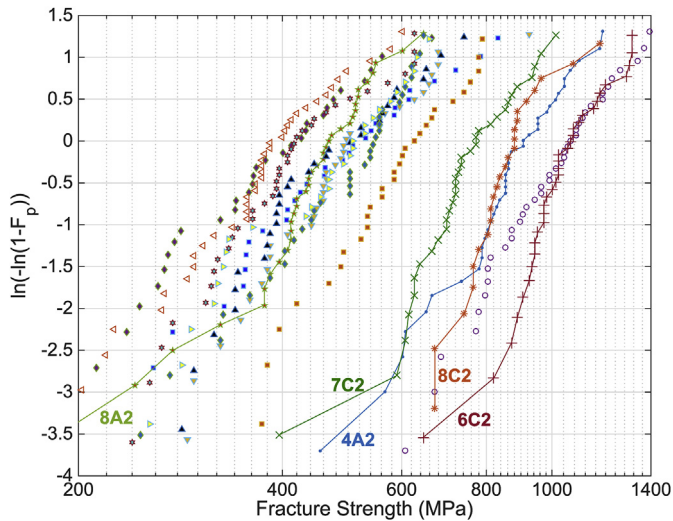


Fig. 10. (a) The hemisphere of the SiC coating layer and (b) the test setup used. Both were adapted from Hunn et al. [48].

Weibull plot in Fig. 11. These range in strength distributions are consistent with other results reported elsewhere [45,46].

Strength data, which were plotted in the Weibull format from select sets in Fig. 11 that span the mid-to-high range of all available data from Hunn et al. [48], were used to calculate the failure probabilities in the simulations of the NSRR experiments. The series were 8C2, 7C2, 6C2, and 4A2, which are from the high-strength group of tested SiC hemisphere samples and 8A2, which is representative of the low-to-average range of the group. Table 4 lists the Weibull parameters for the five selected series. The volume of the full spherical shell was used as the characteristic volume since the local stress, which is the maximum tensile stress on the inner surface near the loading plunger, was scaled onto a full-sized sphere [48].

The loading plunger creates a very small region with very high stresses. However, these local stresses are normalized over the equivalent volume of a sphere to produce the characteristic



**Fig. 11.** Weibull distribution of strength data from SiC hemisphere crush testing. The plot shows a select set of tests performed and adapted from Hunn et al. [48]. Weibull modulus and characteristic strength from five datasets that were plotted as line and markers with their associated IDs were used in the following analyses.

**Table 4**

List of the fracture properties for five of the SiC series [48].

Sample series	Weibull modulus (–)	Characteristic strength (MPa)	Characteristic volume (m <sup>3</sup> )
6C2	7.6	1,101	1.31e-10
7C2	6.1	805	1.40e-10
8C2	8.3	904	1.51e-10
4A2	5.8	1,077	4.5e-11
8A2	4.3	510	9.12e-11

strengths. The corresponding characteristic volume is the volume of the equivalent sphere.

The calculated stress in the SiC shell of the UO<sub>2</sub> TRISO particles in the NSRR tests, which is shown in Fig. 9, was used to assess the failure probability in that coating layer. Since no strength data from the tested particles are available, the Weibull strength parameters from the five selected SiC series in Table 4 were used in Eq. (3) to determine the probability of failure. The results are shown in Fig. 12, and the experimental trend is reproduced from Ref. [6]. While the 8A2 trend predicts higher failure fractions than those observed, it is included on the plot to indicate a best estimate of the failure fractions for an average strength SiC under these conditions.

The shape of the failure probability versus stress is a sigmoid

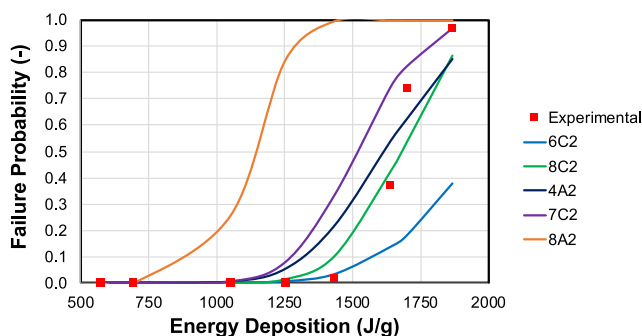


**Fig. 12.** Plot of the predicted failure fractions for the NSRR experiments using a range of SiC fracture parameters. Data reproduced from Ref. [6].

shape, and the effect of increasing the Weibull modulus is to decrease the change in stress to transition from very small to very large failure fractions. The characteristic strength and characteristic volume have similar effects, because they primarily translate the curve to higher or lower stresses. The Weibull modulus for best agreement with the mean failure fractions reported in the NSRR experiments would have been greater than 15. However, this value is significantly outside the range of values typically reported in the literature (–4–8), so data from fracture testing were selected instead.

## 6. Summary and future work

This work simulated a set of historical TRISO particle transient irradiation experiments from NSRR and obtained reasonable agreement in maximum temperature calculations and experimental SiC fracture probability using BISON. This work found that fuel melting is predicted at about the same energy deposition as the onset of SiC fracture. However, the pulse width of the NSRR is short when compared with pulses of other reactors, and it is expected that the onset of fracture for the SiC could occur before fuel melting if wider pulses were used.

A review of mHTGR RIA events in the literature was conducted. The key takeaway from the RIA data is that kernel energy deposition in mHTGRs would likely be less than the lowest fuel kernel energy deposition (578 J/g) in the NSRR experiments. Additionally, the pulse width of an mHTGR CRW would be much greater than the NSRR experiments because of the order-of-magnitude longer neutron generation time in a graphite-moderated system. This conclusion would not be valid for TRISO-fueled systems that used advanced hydride-based moderators, such as Transformational Challenge Reactor (TCR) [49–51]. Although higher-energy depositions can be expected in these systems, it should still remain well below 1,000 J/g. Additionally, the slower speed of a CRW vs. the rapid NSRR transients would impact the timing of the event.

Future work should focus on simulating longer pulses and determining the stresses in other relevant matrix materials, such as SiC [52,53]. Capturing the effects of burnup and fast neutron flux on the kernel and coating layers is another area that needs to be considered. Sensitivity and uncertainty analysis studies of the specific heat, CTE, thermal conductivity, and elastic modulus could also be performed to ascertain the primary governing parameters on behavior of TRISO fuel under transient conditions. Additional future work could include Sobol sensitivity studies of the SiC fracture properties and other simulation parameters.

It is recommended that additional transient tests of TRISO particles be performed to better understand the limits of the TRISO fuel form. Knowing the conditions under which the TRISO fuels will likely fail is far more valuable to the design engineers, regulators, and reactor operators than simply showing that the fuel withstands the expected RIA. The US Nuclear Regulatory Commission supports a more thorough understanding of dynamic fuel service conditions

and corresponding fuel behavior, as well as qualification and assessment of selected fuel performance codes for transient conditions [54].

### Declaration of competing interest

We do not have any conflicts of interest on this project. The authors on this manuscript are employed by Oak Ridge National Laboratory and University of Tennessee and received funding for this work from the Transformational Challenge Reactor project.

### Acknowledgements

The authors acknowledge the BISON and MOOSE code developers for their technical support and the high-performance computing resources made available for this work at Idaho National Laboratory. Aaron Wysocki and Nathan Capps performed a thorough review of the manuscript. This research was supported by the Transformational Challenge Reactor program, US Department of Energy, Office of Nuclear Energy.

### References

- [1] M.T. Simnad, The early history of high-temperature helium gas-cooled nuclear power reactors, *Energy* 16 (1991) 25–32.
- [2] P.A. Demkowicz, B. Liu, J.D. Hunn, Coated particle fuel: historical perspectives and current progress, *J. Nucl. Mater.* 515 (2019) 434–450.
- [3] C.A. Baldwin, J.D. Hunn, R.N. Morris, F.C. Montgomery, C.M. Silva, P.A. Demkowicz, First elevated-temperature performance testing of coated particle fuel compacts from the AGR-1 irradiation experiment, *Nucl. Eng. Des.* 271 (2014) 131–141.
- [4] R.N. Morris, J.D. Hunn, C.A. Baldwin, F.C. Montgomery, T.J. Gerczak, P.A. Demkowicz, Initial results from safety testing of US AGR-2 irradiation test fuel, *Nucl. Eng. Des.* 329 (2018) 124–133.
- [5] D.M. Perez, R.L. Williamson, S.R. Novascone, G. Pastore, J. Hales, B.W. Spencer, Assessment of BISON: a nuclear fuel performance analysis code, Idaho Natl. Lab, Idaho Falls, (2013).
- [6] M. Umeda, T. Sugiyama, F. Nagase, T. Fuketa, S. Ueta, K. Sawa, Behavior of coated fuel particle of high-temperature gas-cooled reactor under reactivity-initiated accident conditions, *J. Nucl. Sci. Technol.* 47 (2010) 991–997.
- [7] K. Terrani, Accelerating advanced nuclear fuel development and qualification: engineering-scale modeling and simulation integrated with separate effects testing, *J. Nucl. Mater.* (2020).
- [8] N.R. Brown, H. Ludewig, A. Aronson, G. Raitses, M. Todosow, Neutronic evaluation of a PWR with fully ceramic microencapsulated fuel. Part II: nodal core calculations and preliminary study of thermal hydraulic feedback, *Ann. Nucl. Energy* 62 (2013) 548–557.
- [9] N.R. Brown, V. Seker, S.T. Revankar, T.J. Downar, Coupling of purdue hydrogen production cycle models to thermix, in: 2007 Int. Top. Meet. Saf. Technol. Nucl. Hydrog. Prod. Control. Manag., 2007, pp. 339–346.
- [10] N.R. Brown, V. Seker, S.T. Revankar, T.J. Downar, An endothermic chemical process facility coupled to a high temperature reactor. Part I: proposed accident scenarios within the chemical plant, *Nucl. Eng. Des.* 246 (2012) 256–265.
- [11] J.C. Cleveland, Modular high-temperature gas-cooled reactor short-term thermal response to flow and reactivity transients, Nuclear Regulatory Commission, Washington, DC (United States), Div. of Systems Research; Oak Ridge National Lab. (1993), <https://doi.org/10.2172/6867065>. <https://search.crossref.org/?q=Modular+high-temperature+gas-cooled+reactor+short-term+thermal+response+to+flow+and+reactivity+transients%2C+Nuclear+Regulatory+Commission%2C+Washington%2C+DC+%28United+States%29>.
- [12] S. Hu, R. Wang, Z. Gao, Transient tests on blower trip and rod removal at the HTR-10, *Nucl. Eng. Des.* 236 (2006) 677–680.
- [13] F. Gou, Y. Liu, F.-B. Chen, Y.-J. Dong, Thermal behavior of the HTR-10 under combined PLOFC and ATWS condition initiated by unscrammed control rod withdrawal, *Nucl. Sci. Tech.* 29 (2018) 123.
- [14] M. Lang, Y. Dong, The ATWS analysis of one control rod withdraw out of the HTR-10GT core in addition with bypass valve failure, *Nucl. Eng. Des.* 271 (2014) 459–464.
- [15] C. Lu, B.D. Hiscox, K.A. Terrani, N.R. Brown, Fully ceramic microencapsulated fuel in prismatic high temperature gas-cooled reactors: analysis of reactor performance and safety characteristics, *Ann. Nucl. Energy* 114 (2018) 277–287.
- [16] S. Nakagawa, K. Takamatsu, Y. Tachibana, N. Sakaba, T. Iyoku, Safety demonstration tests using high temperature engineering test reactor, *Nucl. Eng. Des.* 233 (2004) 301–308.
- [17] J. Ortensi, A.M. Ougouag, Improved Prediction of the Temperature Feedback in TRISO-Fueled Reactors, Idaho National Laboratory (INL), 2009.
- [18] F. Reitsma, Reactivity considerations for the on-line refuelling of a pebble bed modular reactor—illustrating safety for the most reactive core fuel load, *Nucl. Eng. Des.* 251 (2012) 18–29.
- [19] A. Seubert, A. Sureda, J. Bader, J. Lapins, M. Buck, E. Laurien, The 3-D time-dependent transport code TORT-TD and its coupling with the 3D thermal-hydraulic code ATTICA3D for HTGR applications, *Nucl. Eng. Des.* 251 (2012) 173–180.
- [20] G. Strydom, TINTe Transient Results for the OECD 400 MW PBMR Benchmark, Proc. ICAPP '08, Anaheim, USA, 2008.
- [21] G. Strydom, F. Reitsma, P. Ngeleka, K. Ivanov, The OECD/NEA/NSC PBMR 400 MW coupled neutronics thermal hydraulics transient benchmark: transient results. Proc. PHYSOR-2010 Conf, Int. Conf. Phys. React., Pittsburgh, PA, USA, 2010.
- [22] F. Reitsma, G. Strydom, J.B.M. De Haas, K. Ivanov, B. Tyobeka, R. Mphahlele, T.J. Downar, V. Seker, H.D. Gougar, D.F. Da Cruz, The PBMR steady-state and coupled kinetics core thermal-hydraulics benchmark test problems, *Nucl. Eng. Des.* 236 (2006) 657–668.
- [23] Y. Zheng, L. Shi, Reactivity accident due to control rod inadvertent withdrawal of the 250MW high temperature gas-cooled reactor, in: 18th Int. Conf. Nucl. Eng., American Society of Mechanical Engineers Digital Collection, 2010, pp. 337–343.
- [24] Japan Atomic Energy Agency, NSRR, (n.d.). [https://www.jaea.go.jp/english/04/ntokai/kasokuki/kasokuki\\_03.html](https://www.jaea.go.jp/english/04/ntokai/kasokuki/kasokuki_03.html).
- [25] T. Nakamura, S. Katanishi, Y. Kashima, S. Yachi, M. Yoshinaga, Y. Terakado, High power transient characteristics and capability of NSRR, *J. Nucl. Sci. Technol.* 39 (2002) 264–272.
- [26] S. Saito, T. Inabe, T. Fujishiro, N. Ohnishi, T. Hoshi, Measurement and evaluation on pulsing characteristics and experimental capability of NSRR, *J. Nucl. Sci. Technol.* 14 (1977) 226–238.
- [27] M.N. Cinbiz, N.R. Brown, K.A. Terrani, R.R. Lowden, D. Erdman III, A pulse-controlled modified-burst test instrument for accident-tolerant fuel cladding, *Ann. Nucl. Energy* 109 (2017) 396–404.
- [28] C.J. Permann, D.R. Gaston, D. Andrs, R.W. Carlsen, F. Kong, A.D. Lindsay, J.M. Miller, J.W. Peterson, A.E. Slaughter, R.H. Stogner, MOOSE: Enabling Massively Parallel Multiphysics Simulation, 2019. 1911.04488.
- [29] B.S. Kirk, J.W. Peterson, R.H. Stogner, G.F. Carey, libMesh: a C++ library for parallel adaptive mesh refinement/coarsening simulations, *Eng. Comput.* 22 (2006) 237–254.
- [30] S. Abhyankar, J. Brown, E.M. Constantinescu, D. Ghosh, B.F. Smith, H. Zhang, Petsc/ts: a modern scalable ode/dae solver library. 1806.01437, 2018.
- [31] J.D. Hales, R.L. Williamson, S.R. Novascone, D.M. Perez, B.W. Spencer, G. Pastore, Multidimensional multiphysics simulation of TRISO particle fuel, *J. Nucl. Mater.* 443 (2013) 531–543.
- [32] F.H. Ho, Graphite Design Handbook, General Atomics, San Diego, CA (US), 1988.
- [33] F. Cappia, D. Pizzocri, M. Marchetti, A. Schubert, P. Van Uffelen, L. Luzzi, D. Papaioannou, R. Macian-Juan, V.V. Rondinella, Microhardness and Young's modulus of high burn-up UO<sub>2</sub> fuel, *J. Nucl. Mater.* 479 (2016) 447–454.
- [34] L.L. Snead, T. Nozawa, Y. Katoh, T.-S. Byun, S. Kondo, D.A. Petti, Handbook of SiC properties for fuel performance modeling, *J. Nucl. Mater.* 371 (2007) 329–377.
- [35] D. Petti, P. Martin, M. Phelp, R. Ballinger, Development of Improved Models and Designs for Coated-Particle Gas Reactor Fuels—Final Report under the International Nuclear Energy Research Initiative (I-NERI), Idaho National Lab.(INL), Idaho Falls, ID (United States); Centre d'Etude Atomique (CEA), Saclay (France); Massachusetts Inst. Of Technology (MIT), Cambridge, MA (United States) INEEL/EXT-05-02615, 2004.
- [36] J.K. Fink, Thermophysical properties of uranium dioxide, *J. Nucl. Mater.* 279 (2000) 1–18.
- [37] J.J. Powers, TRISO Fuel Performance: Modeling, Integration into Mainstream Design Studies, and Application to a Thorium-Fueled Fusion-Fission Hybrid Blanket, Lawrence Livermore National Lab.(LLNL), Livermore, CA (United States), 2011. LLNL-TR-517411.
- [38] M. Li, N. V Mokhov, Experience with Moving from Dpa to Changes in Materials Properties, ANL, Fermilab, Morschach, Switzerland, Present, 2010.
- [39] J.K. Hohorst, SCDAP/RELAP5/MOD2 code manual, volume 4: MATPRO—a library of materials properties for light-water-reactor accident analysis, EG&G Idaho Rep. NUREG/CR (1990) 5273.
- [40] D.G. Martin, The thermal expansion of solid UO<sub>2</sub> and (U, Pu) mixed oxides—a review and recommendations, *J. Nucl. Mater.* 152 (1988) 94–101.
- [41] K. Fukuda, T. Ogaw, K. Hayashi, S. Shiozawa, H. Tsuruta, I. Tanaka, N. Suzuki, S. Yoshimuta, M. Kaneko, Research and development of HTTR coated particle fuel, *J. Nucl. Sci. Technol.* 28 (1991) 570–581.
- [42] W.J. Kim, J.N. Park, M.S. Cho, J.Y. Park, Fracture Strength of Silicon Carbide Layers of TRISO Particles Coated at Various Temperatures, 2008.
- [43] S. Hong, T. Byun, R.A. Lowden, L.L. Snead, Y. Katoh, Evaluation of the fracture strength for silicon carbide layers in the tri-isotropic-coated fuel particle, *J. Am. Ceram. Soc.* 90 (2007) 184–191.
- [44] P. Hosemann, J.N. Martos, D. Frazer, G. Vasudevamurthy, T.S. Byun, J.D. Hunn, B.C. Jolly, K. Terrani, M. Okuniewski, Mechanical characteristics of SiC coating layer in TRISO fuel particles, *J. Nucl. Mater.* 442 (2013) 133–142.
- [45] N. Rohbeck, P. Xiao, Evaluation of the mechanical performance of silicon carbide in TRISO fuel at high temperatures, *Nucl. Eng. Des.* 306 (2016) 52–58.
- [46] X. Xie, B. Liu, Y. Guo, R. Liu, X. Zhao, N. Ni, F. Guo, P. Xiao, Effect of hydrothermal corrosion on the fracture strength of SiC layer in tristructural-



- isotropic fuel particles, *J. Am. Ceram. Soc.* (n.d.).
- [47] N. Rohbeck, P. Xiao, Effects of thermal treatment on the mechanical integrity of silicon carbide in HTR fuel up to 2200° C, *J. Nucl. Mater.* 451 (2014) 168–178.
  - [48] J.D. Hunn, T.S. Byun, J.H. Miller, Fabrication and Characterization of Sixteen SiC Variants Deposited on the Same IPyC Substrate for Fracture Strength Testing, Oak Ridge Natl. Lab. Res. Report. ORNL/TM-2009/324, 2009.
  - [49] B.R. Betzler, B.J. Ade, A.J. Wysocki, M.S. Greenwood, K.G. Field, J.M. Risner, P.K. Jain, J.R. Burns, B.D. Hiscox, Transformational Challenge Reactor Pre-conceptual Design Incorporating Rapid Prototyping via Advanced Manufacturing, 2018 <https://doi.org/ORNL/SPR-2018/1008>.
  - [50] B. Ade, A. Wysocki, B. Betzler, M. Greenwood, P. Chesser, P. Jain, J. Burns, K. Terrani, J. Rader, B. Hiscox, J. Heineman, J. Risner, K. Smith, F. Heidet, A. Bergeron, J. Sterbentz, T. Holschuh, Candidate core designs for the transformational Challenge reactor, in: *PHYSOR 2020*, Cambridge, 2020.
  - [51] Oak Ridge National Laboratory, Transformational Challenge reactor, (n.d.), <https://tcr.ornl.gov/>.
  - [52] K.A. Terrani, J.O. Kiggans, Y. Katoh, K. Shimoda, F.C. Montgomery, B.L. Armstrong, C.M. Parish, T. Hinoki, J.D. Hunn, L.L. Snead, Fabrication and characterization of fully ceramic microencapsulated fuels, *J. Nucl. Mater.* 426 (2012) 268–276.
  - [53] D. Schappel, K. Terrani, J.J. Powers, L.L. Snead, B.D. Wirth, Modeling the performance of TRISO-based fully ceramic matrix (FCM) fuel in an LWR environment using BISON, *Nucl. Eng. Des.* 335 (2018) 116–127.
  - [54] US Nuclear Regulatory Commission, Assessment of White Paper Submittals of Fuel Qualification and Mechanistic Source Terms (Revision 1), Next Generation Nuclear Plant, ML14174A845, 2014.